

# The Local Oxygen Transport Resistance of Ultra-Low Platinum Loading Cathode Catalyst Layer

Kuangwei Cheng<sup>1,2</sup>, Shang Li<sup>1,2,\*</sup>, Kang Hong<sup>1</sup>, Zhiyong Wen<sup>1</sup>, Zhen Zhu<sup>1,2</sup>, Wei Yan<sup>1</sup>, Mu Pan<sup>1,2</sup>

<sup>1</sup> State Key Laboratory of Advanced Technology for Materials Synthesis and Processing, Wuhan University of Technology, Luoshi Road 122#, Wuhan 430070, PR China

<sup>2</sup> Foshan Xianhu Laboratory of the Advanced Energy Science and Technology Guangdong Laboratory, Xianhu Hydrogen

\*E-mail: [lishang@whut.edu.cn](mailto:lishang@whut.edu.cn)

Received: 9 January 2022 / Accepted: 15 February 2022 / Published: 5 April 2022

---

This study aims at the problem of the lower performance of membrane electrode assembly with the decrease in platinum loading in proton exchange membrane fuel cells. The local oxygen transport resistances of 30wt.%Pt/C catalyst layer and 60wt.%Pt/C carbon-doped dilution catalyst layers were calculated and compared by limiting the current density test. During this process, the total mass transfer resistance was replaced by pressure-independent oxygen transport resistance to eliminate the effect of pressure-dependent mass transfer resistance, thus, Knudsen diffusion resistances in the catalyst layer and microporous layer were considered. Results showed that 60wt.%Pt/C carbon-doped dilution catalyst layer exhibited higher bulk phase Knudsen diffusion resistance and local oxygen transport resistance than that of 30wt.%Pt/C catalyst layer, thereby, decreasing the performance at high current density. In addition, the reasons for lower performance were also analyzed.

---

**Keywords:** Proton exchange membrane fuel cells; Membrane electrode assembly; Cathode catalyst layer; Local oxygen transport resistance; Carbon-doped dilution

## 1. INTRODUCTION

Proton exchange membrane fuel cells (PEMFCs) have remarkable advantages of high energy utilization efficiency, environment friendliness, and thus possess broad application prospects [1-4]. However, the high cost of PEMFCs is one of the important factors limiting their commercial application [5], attributed to the high loading of noble metal catalyst required for high cathode oxygen reaction reduction (ORR) overpotential [6-8]. Reducing the platinum loading of the cathode catalyst layer (CCL) has an increasingly vital role in the commercialization of PEMFCs.

However, several recent studies have demonstrated that with the decrease in platinum loading the performance of membrane electrode assembly (MEA) substantially decreases [3,10-13,15]. Kongkanand et al. tested the single-cell polarization curves (I-V) of PtCo/C catalysts with different loadings ( $0.2\text{mg}_{\text{Pt}}/\text{cm}^2$ ,  $0.1\text{mg}_{\text{Pt}}/\text{cm}^2$ , and  $0.05\text{mg}_{\text{Pt}}/\text{cm}^2$ ) and observed the unaccounted voltage loss at high current density [3]. Ono et al. demonstrated that decreased Pt-loading drastically increased the voltage loss of the cathode catalyst layer (CCL) at high current density. According to the modified 1-D calculation model, they speculated  $R_{O_2, \text{CCL}-\text{micro}}$  was a dominant factor responsible for this loss [9]. Owejan et al. controlled the Pt loading of the CCL ranging from  $0.025\text{mg}_{\text{Pt}}/\text{cm}^2$  to  $0.3\text{mg}_{\text{Pt}}/\text{cm}^2$  using bare Vulcan carbon-doped dilution [10]. The I-V results showed that the performance of the single fuel cell dramatically decreased with the decrease in platinum loadings. They concluded that the higher total transport resistance of 60% Pt/C carbon-doped dilution CCL was responsible for the performance degradation compared with undiluted CCL with 30% Pt/C. Furthermore, they demonstrated that this performance difference was attributed to the interface between platinum and ionomer surrounding the catalyst-layer agglomerates. By simulating the current density of a single Pt particle, the physical source of transport resistance was further analyzed. It was revealed that the oxygen transport resistance (OTR) of the gas/ionomer interface and Pt/ionomer interface both were prominent factors affecting the performance of different wt.%Pt/C ratio catalysts. However, the local oxygen transport resistance ( $R_{O_2}^{\text{Pt}}$ ) of the two electrodes was not measured. Makharia et al. explored the relationship between  $R_{O_2}^{\text{Pt}}$  and platinum loading. They demonstrated that the  $R_{O_2}^{\text{Pt}}$  increased exponentially with decreasing platinum loading [11]. Nonoyama et al. quantified the OTR of each fuel-cell layer by limiting-current density measurements. They found that the oxygen resistance through ionomer increased with the decrease in platinum loading or temperature [12]. Based on Henry's law, the formula for oxygen concentration related to oxygen partial pressure at the interface between gas and ionomer was deduced by Kudo et al. [13]. However, this formula only expresses the pressure-related transmission resistance; there is more pressure-independent transport resistance in the catalyst layer. Liu et al. measured proton conduction resistance of different MEA with various ionomer/carbon weight ratios, characterized by the AC impedance at different relative humidity, and concluded that the  $R_{O_2}^{\text{Pt}}$  of CCL is strongly correlated with humidity [14]. Greszler et al. prepared CCL with different platinum loadings in the range of  $0.03\text{-}0.4\text{mg}_{\text{Pt}}/\text{cm}^2$  by doping 50% Pt/C catalyst with Vulcan bare carbon under fixed electrode thickness and deduced the reciprocal relation between total transport resistance ( $R_{\text{tot}}$ ) and platinum loading. As a result, they proposed that the  $R_{O_2}^{\text{Pt}}$  was obtained by measuring the  $R_{\text{electrode}}$  by different low-platinum-loading CCL [15]. Based on these analyses, with the decrease in platinum loading, the performance of the membrane electrode decreased significantly, mainly attributed to the increased transport OTR in the catalyst layer. Therefore, it is significant to study the OTR of low Pt-loaded CCL with different structure to optimize the structure of CCL and improve its performance.

In this study, the limiting current density method is used to measure the  $R_{O_2}^{\text{Pt}}$  in two electrode structures, i.e., 30wt.%Pt/C catalyst without dilution and 60wt.%Pt/C one with carbon-doped dilution, and the reasons for the performance change in two electrodes are elucidated.

## 2. THEORY

The deduction process of local oxygen transport resistance theory is based on the theoretical analysis of Baker [16] and Greszler [15]. In general, the calculation of  $R_{O_2}^{Pt}$  under specific structure catalyst layer is divided into following two steps:

(1) The limiting current density ( $I_{lim}$ ) of as-mentioned CL at three loadings was measured and  $R_{tot}$  was calculated;

(2) According to cyclic voltammetry curve (CV) results, the electrochemical active surface area (ECSA) was calculated to obtain the corresponding roughness factor ( $f_{Pt}$ ), and local mass transfer resistance was obtained by linear fitting between  $R_{total}$  and  $1/f_{Pt}$ .

According to Eq.1 derived by Baker et al. [16], the  $R_{tot}$  under different loadings can be calculated according to  $I_{lim}$ :

$$R_{tot} = \frac{4Fx_{O_2}(P_{abs}-P_{H_2O})}{RTI_{lim}} \quad (1)$$

where  $F$  is Faraday constant,  $x_{O_2}$  represents dry oxygen mole fraction,  $T$  indicates the absolute cell temperature,  $R$  is the universal gas constant,  $P_{abs}$  represents the absolute gas pressure, and  $P_{H_2O}$  is the water vapor pressure.

According to Eq. 2 derived by Greszler et al. [15] :

$$R_{tot} = R_{CH} + R_{DM} + R_{MPL} + \frac{R_{O_2}^{Pt}}{f_{Pt}} \quad (2)$$

where  $R_{CH}$ ,  $R_{DM}$  and  $R_{MPL}$  are the oxygen transport resistances in channels of flow field plate, diffusion media, and micro-porous layer, respectively,  $R_{O_2}^{Pt}$  denotes local oxygen transport resistance of single Pt particle,  $f_{Pt}$  is the roughness factor equal to the product of platinum loading  $L_{Pt}$  in mass per unit geometric electrode area and the electrochemical effective surface area  $A_{Pt}$  per unit mass of platinum, that is,  $f_{Pt} = L_{Pt} \times A_{Pt}$  [15,17]. Considering that the bulk transport resistance ( $R_{bulk}$ ) of CL with low-Pt-loading accounted for a higher proportion of  $R_{total}$  [18], the Eq. 2 should be corrected as Eq.3:

$$R_{tot} = R_{CH} + R_{DM} + R_{MPL} + R_{bulk} + \frac{R_{O_2}^{Pt}}{f_{Pt}} \quad (3)$$

where the oxygen transfer resistance of catalyst layer and microporous layer is further divided into Knudsen diffusion resistance and molecular diffusion resistance:

$$R_{MPL} = R_{MPL-Molecular} + R_{MPL-Knudsen} \quad (4)$$

$$R_{bulk} = R_{CL-Molecular} + R_{CL-Knudsen} \quad (5)$$

And then, Eq.6 is obtained by substituting Eq.4 and 5 to Eq.3:

$$R_{tot} = R_{CH} + R_{DM} + R_{MPL-Molecular} + R_{MPL-knudsen} + R_{CL-Molecular} + R_{CL-knudsen} + \frac{R_{O_2}^{Pt}}{f_{Pt}} \quad (6)$$

According to the relative pore size value and the average free path of gas molecules, the  $R_{tot}$  is further divided into pressure-dependent parts ( $R_P$ ) and pressure-independent part ( $R_{NP}$ ) [19]. Then  $R_{tot}$  also is expressed as Eq.7:

$$R_{tot} = R_{NP} + R_P \quad (7)$$

where,

$$R_P = R_{CH} + R_{GDB} + R_{MPL-Molecular} + R_{CL-Molecular} \quad (8)$$

Thereupon, Eq. 2 is acquired by substituting Eq. 6 from Eq. 8:

$$R_{NP} = R_{total} - R_P = R_{MPL-Knudsen} + R_{CL-Knudsen} + \frac{R_{O_2}^{Pt}}{f_{Pt}} \quad (9)$$

Herein, the same GDL is used for two membrane electrode assemblies (MEAs) with different Pt-loadings, and thus  $R_{MPL-Knudsen}$  is constant. Besides, the preparation of CCL with different platinum loading is the same, and the platinum loading of MEA changes by increasing the thickness of CCL. We assume that the  $R_{bulk}$  of as-mentioned CCL is constant, and then  $R_{CL-knudsen}$  should be constant. Therefore, the  $R_{total}$  has a linear relation with  $1/f_{Pt}$  and the slope of the fitting line is  $R_{O_2}^{Pt}$ . By calculating ECSA of CCL with three low-Pt-loadings [20], the corresponding  $f_{Pt}$  is calculated, hence, the slope fitted by  $1/f_{Pt}$  on  $R_{NP}$  is  $R_{O_2}^{Pt}$ .

### 3. EXPERIMENT AND CHARACTERIZATION

#### 3.1 Preparation of MEA

The catalyst layers with different structures were prepared using 30wt.%Pt/C and 60wt.%Pt/C catalysts (TKK), respectively. The catalyst ink-1 was composed of 30wt.% Pt/C catalyst, isopropyl alcohol, deionized water (resistivity  $\geq 18.25 \text{ M}\Omega \text{ cm}$ ), and 5wt.% Nafion (PFSA) solution. The catalyst ink-2 contained all the as-mentioned components apart from Vulcan XC-72 to dilute 60wt.%Pt/C to 30wt.% Pt/C. And then the as-prepared catalyst pastes were blade coated on PTFE film to form CCL, followed by the decal-transfer on  $15\mu\text{m}$  proton exchange membrane (Gore) to fabricate different loading MEA (MEA-1-0.06  $\text{mg}/\text{cm}^2$ , MEA-1-0.116  $\text{mg}/\text{cm}^2$ , MEA-1-0.152  $\text{mg}/\text{cm}^2$ , MEA-2-0.08  $\text{mg}/\text{cm}^2$ , MEA-2-0.119  $\text{mg}/\text{cm}^2$ , and MEA-2-0.156  $\text{mg}/\text{cm}^2$ ). MEA-1 and MEA-2 were fabricated by catalyst ink-1 and ink-2, respectively; those MEAs were named after different Pt-loading (0.06  $\text{mg}/\text{cm}^2$ , 0.116  $\text{mg}/\text{cm}^2$ , 0.152  $\text{mg}/\text{cm}^2$ , 0.08  $\text{mg}/\text{cm}^2$ , 0.119  $\text{mg}/\text{cm}^2$ , 0.156  $\text{mg}/\text{cm}^2$ ). Their active areas were designed for I-V and OTR tests, corresponding to  $5\times 5 \text{ cm}^2$  or  $1\times 2 \text{ cm}^2$ , respectively. The Pt loading of the anode was 0.1  $\text{mg}/\text{cm}^2$  and the catalyst loading of CCL with different MEAs is listed in Table 2.

#### 3.2 Morphology characterization

To observe the cross-section morphology of as-prepared CCL at 0.1  $\text{mg}/\text{cm}^2$  Pt loading, the corresponding MEA sample was cooled in liquid nitrogen for 3 min, followed by breaking with tweezers and then characterized by scanning electron microscopy (SEM, JSM-7500F).

#### 3.3 Polarization curves

The polarization curves test was the same as reported in our previous research [21]. After activating the single-cell at 0.5 V for 2 h, the stoichiometry of anode and cathode was set at 2.0 in fuel cell test stand (Scribner Associates 890E, HEPHAS), the relative humidity (RH) was 70%, the single-cell temperature was set at  $75 \text{ }^\circ\text{C}$ , and the outlet back pressure was 150 KPa.

### 3.4 Cyclic voltammetry curves

Cyclic voltammetry (CV) data were recorded after I-V curve measurements. The anode/cathode were simultaneously purged with hydrogen and nitrogen, respectively, till the output voltage of sing-cell was reduced to sub-0.1 V. The gas flow rates of anode and cathode were maintained at 200 mL/min during the experiment. The outlet backpressure of the cathode and anode both were ambient pressure. The temperature of the sing-cell, anode, and cathode gas was 30 °C and the relative humidity was 100%.

### 3.5 Limiting current density

The limiting current densities of different loadings MEAs were measured on the same test station with the I-V test under the conditions of hydrogen entering the anode and nitrogen-diluted oxygen entering the cathode, as described by Wan et al [22]. The micro-cell voltage range was 0.7 ~ 0.0 V, and the current density at 0.05 V was taken as  $I_{lim}$ . The specific test conditions are shown in Table 1.

**Table 1.** Test condition for limiting current density

Test condition	HEPHATS(HTS-125)
Cell temperature/°C	75
Relative humidity	70%
Gas absolute pressure/KPa	100 150 200 250
Dry oxygen mole fraction/%	0.5 1 2 4
Anode flow rate (mL/min)	1800
Cathode flow rate (mL/min)	4600

## 4. RESULTS AND DISCUSSION

### 4.1 Characterization of the thickness of CCL

Figure 1-(a) and 1-(b) show the SEM cross-section morphologies of MEA-1-0.116 and MEA-2-0.119 samples, respectively. The thickness of the CCL of the two MEAs is almost similar, and the thicknesses of the samples MEA-1-0.116 and MEA-2-0.119 are 4.1  $\mu\text{m}$  and 4.2  $\mu\text{m}$ , respectively, as shown in Figure 1. However, the difference between both samples is the different distribution of Pt particles, as shown in schematic diagram 2, and this hypothesis is confirmed by Owejan et al. [10] and Nonoyama et al. [12]. In the undiluted CCL, each carbon particle is loaded with platinum particles, and these platinum particles are evenly distributed in the catalyst layer, while in the carbon-doped diluted catalyst layer, Pt particles are unevenly distributed. This structural difference can affect the performance. Preparation conditions and specification parameters are listed in Table 2. The thickness of CCL prepared in our experiment is close to that of Ono et al. [6], about 1/3 of that prepared by Greszler et al. [15]. The thickness of CCL prepared by Greszler et al. is higher than our counterparts, due to higher carbon dilution factor, resulting in more diluted carbon in CCL.

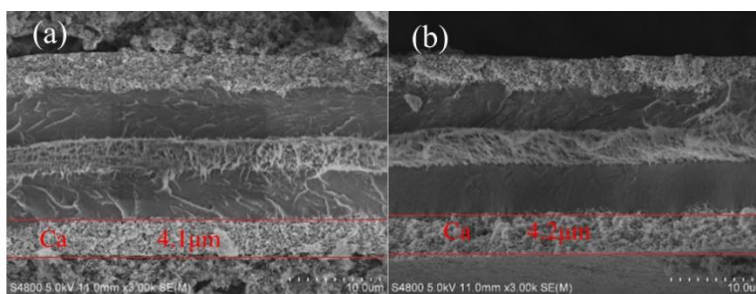


**Figure 1.** Freeze-fractured SEM images of different structures MEA at 3K magnification: (a) SEM cross-section morphology of MEA-1-0.116 sample and (b) MEA-2-0.119 sample.

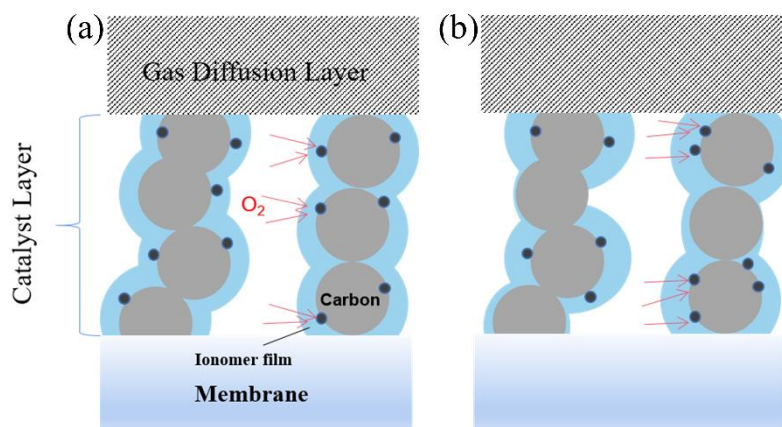


**Figure 2.** Schematic diagram of platinum and ionomer distribution in different structural CCL: (a) Evenly distributed ionomer surrounding Pt-loading CCL and (b) unevenly distribution ionomer surrounding Pt-loading-carbon and bare carbon power.

**Table 2.** The thickness of CCL reported by different research teams

Research team	Cathode Loading (mg Pt/cm <sup>2</sup> <sub>geo</sub> )	Dilution Factor (g Catalyst: g Carbon)	Thickness (μm)	Roughness Factor (cm <sup>2</sup> <sub>Pt</sub> /cm <sup>2</sup> <sub>geo</sub> )	Preparation Condition
Greszler et al. [15]	0.1	0.72:1	11.3	60	145°C /2 min /1.5 MPa
Ono et al. [6]	0.12	1:0	3.8	/	150°C/10 min /0.8 MPa
This work (30%)	0.116	1:0	4.1	68.1905	150°C /3 min /0.8 MPa
This work (60%-30%)	0.119	1:1	4.2	77.9998	150°C /3 min /0.8 MPa

#### 4.2 Polarization Curve

Figure 3 shows the I-V curves of MEA-1-0.116 mg/cm<sup>2</sup> and MEA-2-0.119 mg/cm<sup>2</sup>. Under low current density, the current density vs. voltage (I-V) curves and current density vs. power density (I-P) curves of MEA-1-0.116 mg/cm<sup>2</sup> and MEA-2-0.119 mg/cm<sup>2</sup> coincide with each other. In a high current density region, when current density increased to 1500 mA/cm<sup>2</sup>, the performance of the latter is lower than that of the former, suggesting that the carbon-doped CCL has a large concentration overpotential loss, consistent with the previous results [10]. As mentioned in reference [4], this is attributed to the

increase in OTR of the carbon-doped catalyst layer which accordingly leads to the greater concentration polarization.

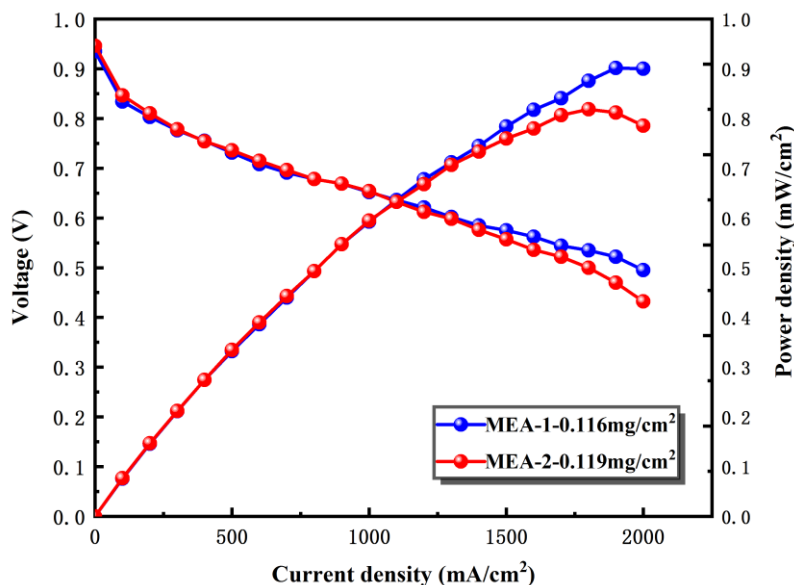


**Figure 3.** I-V curves of MEA-1-0.116 mg/cm<sup>2</sup> and MEA-2-0.119 mg/cm<sup>2</sup> at 70% RH and 150 KPa.

#### 4.3 Local oxygen transport resistance of CCL

Figure 3-(a-c) shows the change in limiting current density of MEA-1 with oxygen mole fraction under three platinum loading, that is, 0.06 mg/cm<sup>2</sup>, 0.116 mg/cm<sup>2</sup> and 0.152 mg/cm<sup>2</sup>. According to theory analysis in Section 2, the slope of the line obtained by linear fitting based on Eq.1 is the value of  $R_{tot}$  under different pressures. And then  $R_{tot}$  is plotted and fitted to the absolute pressure to obtain a straight line, and its intercept is pressure-independent oxygen mass transfer resistance ( $R_{NP}$ ), as shown in Figure 3-(d-f). Using the same method, the limiting current density and  $R_{tot}$ -pressure diagram of MEA-2 with dry oxygen mole fraction are obtained under three platinum loading conditions of 0.08 mg/cm<sup>2</sup>, 0.119 mg/cm<sup>2</sup>, and 0.156 mg/cm<sup>2</sup> (Figure 4), and the  $R_{NP}$  of MEA-1 is obtained by linearly fitting results. Furthermore, according to CV curves under different loadings (Figure 5), ECSA, roughness factor ( $f_{Pt}$ ), and reciprocal roughness ( $1/f_{Pt}$ ) values of corresponding loadings are calculated and shown in Figure 5. Those fitted and calculated values, i.e.,  $R_{NP}$ , ECSA,  $f_{Pt}$ , and  $1/f_{Pt}$  of MEA-1 and MEA-2 under different loadings of platinum are listed in Table 3.

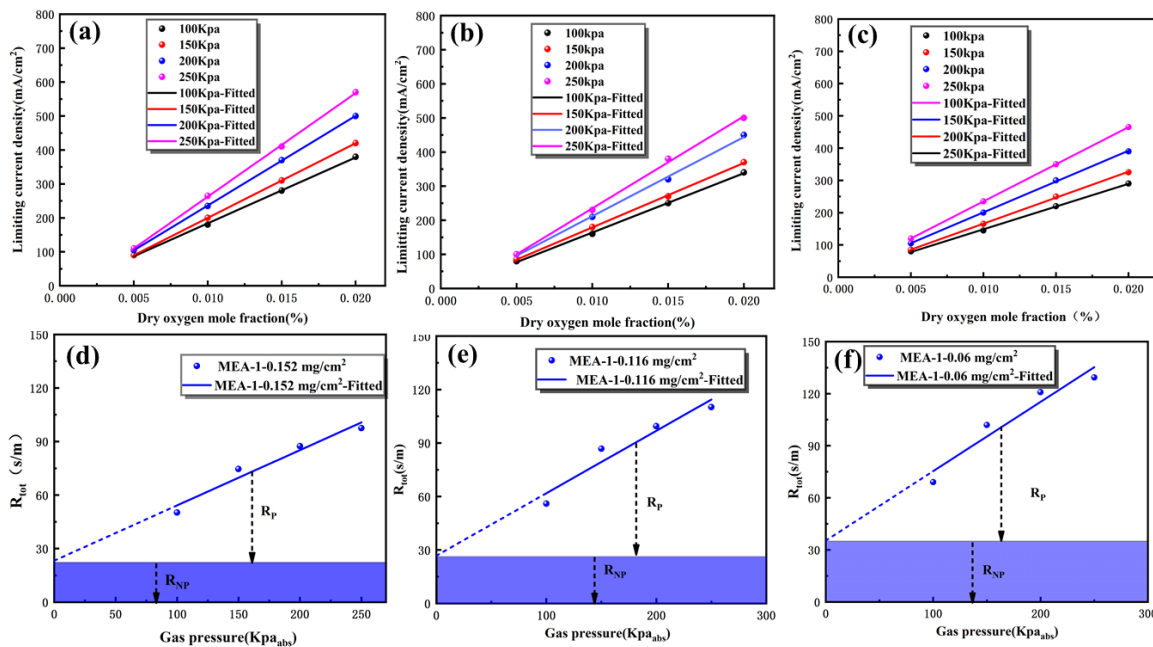


**Figure 3.** The limiting MEA current density of MEA-1 varies with the molar fraction of dry oxygen and the corresponding total mass transfer resistance varies with absolute pressure.

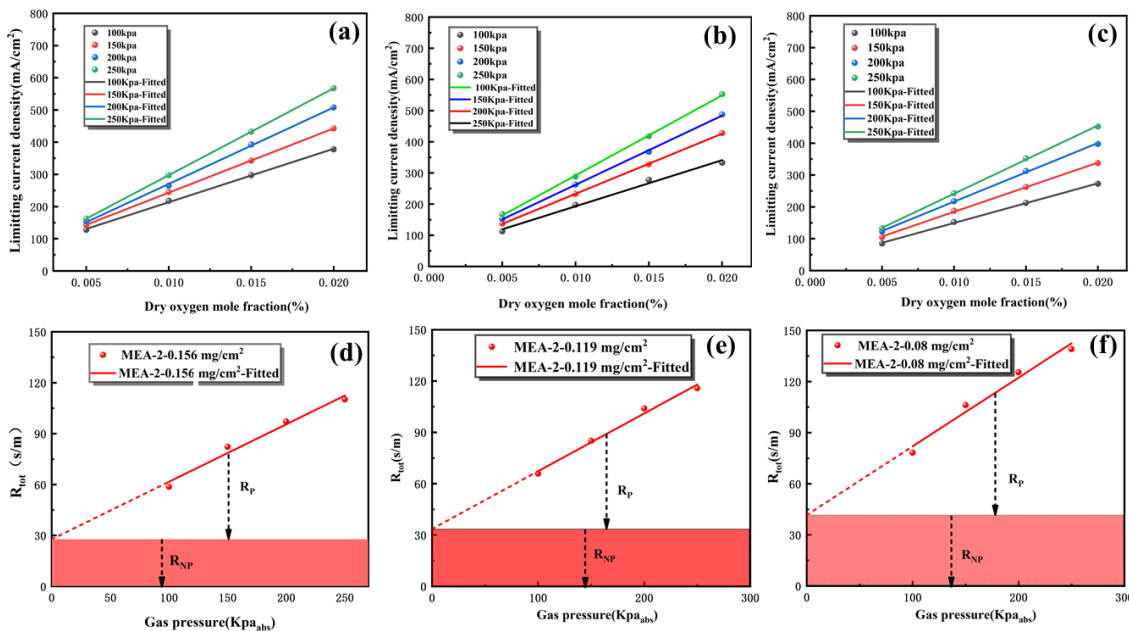


**Figure 4.** The limiting MEA current density of MEA-2 varies with the molar fraction of dry oxygen and the corresponding total mass transfer resistance varies with absolute pressure.

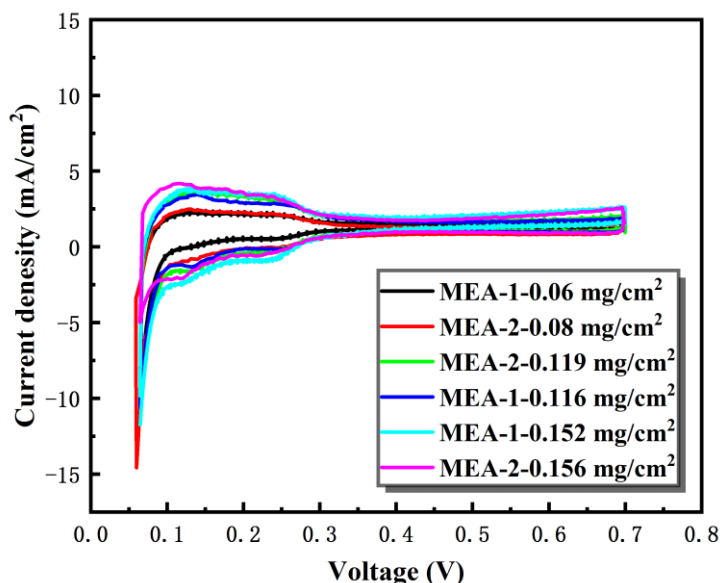


**Figure 5.** The cyclic voltammety curves of CCL with different structures (MEA-1 and MEA-2) at different Pt loadings.

**Table 3.** Electrochemical active surface area and roughness factor of different structural CCL under different loadings.

Sample No.	Platinum loading/(mg/cm <sup>2</sup> )	ECSA/(m <sup>2</sup> /g)	f <sub>Pt</sub>	1/f <sub>Pt</sub>	R <sub>NP</sub> /(s/m)
MEA-1	0.06	56.3492	33.8095	0.0295	35.3765
	0.116	58.7849	68.1905	0.01466	26.7543
	0.152	51.5038	78.2857	0.01277	23.2345
MEA-2	0.08	64.4048	51.5238	0.0194	41.6520
	0.119	65.5462	77.9998	0.0128	33.5492
	0.156	61.0961	97.1429	0.01029	27.7535

Using the data in Table 2,  $R_{NP}$  against  $1/f_{Pt}$  is plotted as a straight line in Figure 6. According to Eq. 9, the slope of linear fitting in Figure 6 is  $R_{O_2}^{Pt}$  of the catalyst layer. The slopes of fitting-lines  $Y_1$  and  $Y_2$  correspond to  $R_{O_2}^{Pt}$  of MEA-1 carbon-diluted sample (13.39 s/cm) and MEA-2 undiluted sample (14.65s/cm), respectively. The latter is 9.41% higher than the former, due to the uneven distribution of Pt particles, causing uneven distribution of PFSA ionomer in CCL. Specifically, the ionomer with sulfonate on the side chain is more likely to adsorb on the surface of Pt catalyst [17], resulting in the selective adsorption of ionomer, preferring adsorbing on the carbon carrier loaded with platinum to bare Vulcan XC-72 without platinum loading. Thicker and denser ionomer films are formed on the surface of the former than the latter. Consequently, the distribution of ionomer surrounding the carbon carrier in the undiluted catalyst layer (MEA-1) is more uniform than the diluted one (MEA-2), as shown in Figure 2. In addition, the intercepts of fitting lines  $Y_1$  and  $Y_2$  correspond to the Knudsen diffusion resistance of the bulk phase in the catalyst layer and the microporous layer of two MEA structures, which are 6.567

s/m and 13.567 s/m, respectively, MEA-2 is 2.06 times of MEA-1. This is attributed to the addition of pure Vulcan XC-72, which increases the tortuosity of gas transport to the three-phase interface to take part in ORR. Greszler et al. adopted  $R_{tot}$  as the calculation basis of  $R_{O_2}^{Pt}$ , and ignored the bulk transfer resistance of the catalyst layer [15], which is debatable. From this perspective,  $R_{NP}$  is used as a calculation basis instead of  $R_{tot}$  to eliminate the effect of pressure-related mass transport resistance in the catalyst layer and consider Knudsen diffusion in the catalyst layer is more reasonable. The above analysis indicates that the higher Knudsen diffusion of bulk phase and local oxygen transport resistance in the catalyst layer both are responsible for the better performance of carbon-doped MEA-2 at high current density compared with MEA-1.

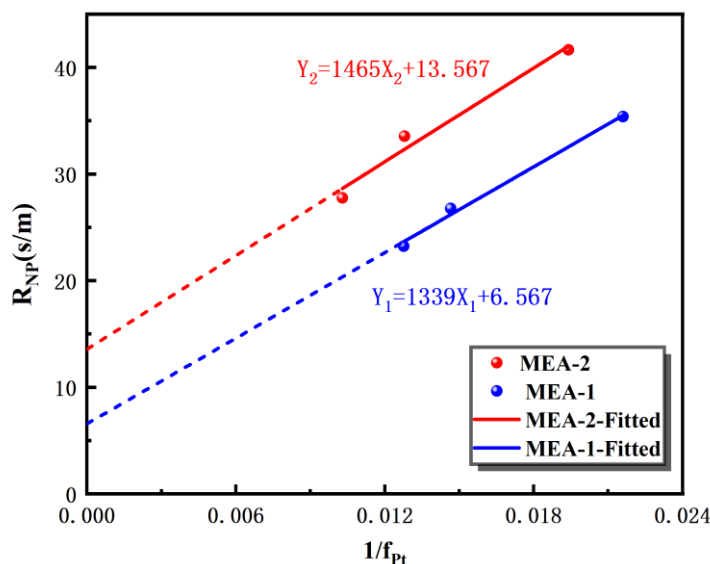


**Figure 6.**  $R_{NP}$  of two structures (MEA-1 and MEA-2) varies with  $1/f_{Pt}$

**Table 4.** Summarized data of local oxygen transport resistance measured by different research groups

Research Group	Low Estimate (s/cm)	High Estimate (s/cm)	Method
Kudo et al. [23]	17	100	Ex-situ
Ono et al. [9]	18	20	In-situ
Greszler et al. [15]	10	17	In-situ
This work (60%-30%)		14.65	In-situ
This work (30%)		13.39	In-situ

Table 4 shows the local transport resistances measured by different research teams. Although the above different results are based on theoretical calculation and in-situ test respectively, they are still comparable due to a relatively close local oxygen transfer process to some extent. Besides, these studies

are classified as in-situ (limiting current density) or ex-situ based on whether they are tested by limiting current density method (reference 13). In addition, the measurements results of this study are relatively closer to the low estimate value of Kudo et al. [23], far from their high estimate, due to different test techniques. Moreover, the larger deviation from the experimental results of Ono et al. [9] and this work is attributed to the higher I/C ratio (0.9) and catalyst layer thickness (11  $\mu\text{m}$ ) used in the former calculations of the 1-D model [24]. Whereas the results obtained in this study are in close agreement with those of Greszler et al. [15] with more precision and resolution for two structures CCL, considering the structure discrepancy of CCL (Table 2), owned to almost identical theory analysis process of  $R_{O_2}^{Pt}$ . In general, this developed method for calculating  $R_{O_2}^{Pt}$  has high reliability and better resolution for different structures CCL.

## 5. CONCLUSION

In this study, the pressure-independent mass transfer resistance was used to replace the total mass transfer resistance as the theoretical analysis basis of local mass transfer resistance, and the Knudsen diffusion resistance in the CL and the MPL was considered. Based on the as-acquired equation, the local mass transfer resistances of 30wt.% Pt/C catalyst layer (MEA-1) and 60wt.% Pt/C carbon-doped dilution catalyst layer (MEA-2) with low platinum loading was calculated and compared. Results showed that the CCL with 60wt.% Pt/C and carbon-doped exhibited higher Knudsen diffusion resistance and local oxygen transport resistance than the catalyst layer with 30wt.% Pt/C and without carbon-doped dilution. The Knudsen diffusion resistance of MEA-2 was 2.06 times of MEA-1 and the local oxygen mass transfer resistance of MEA-2 was 9.41% higher than MEA-1, responsible for lower performance under high current density. This was attributed to the uneven distribution of Platinum in different structural catalyst layers, leading to uneven distribution of the ionomer. The thicker ionomer layer on the surface of the catalysts in high-Pt-loading CCL resulted in a high local oxygen transport resistance. In the catalyst layer with 60wt.% Pt/C doped with Vulcan XC-72, the increase in oxygen transport channel tortuosity was responsible for the greater Knudsen diffusion resistance. Compared with previously reported experimental results, the developed calculation method for local oxygen transport resistance has the advantages of higher reliability and better resolution.

## ACKNOWLEDGEMENTS

This work was financially supported by Foshan Xianhu Laboratory of the Advanced Energy Science and Technology Guangdong Laboratory (Program No. XHD2020-002-03).

## References

1. C. Wang, S. Wang, L. Peng, J. Zhang, Z. Shao, J. Huang, C. Sun, M. Ouyang and X. He, *Energies*, 9 (2016) 603.
2. D. Banham, T. Kishimoto, Y. Zhou, T. Sato, K. Bai, J.I. Ozaki, Y. Imashiro, S. Ye, *Science Advances*, 4 (2018) 71–80.
3. A. Kongkanand, M.F. Matias, ASME 8th International Fuel Cell Science, Engineering & Technology Conference: Brooklyn, NY, (2010).

4. H. Liu, X. Xing, W. Shang, T. Li, *International Journal of Electrochemical Science*, 16 (2021) 1–16.
5. T. Sadhasivam, K. Dhanabalan, S.H. Roh, T.H. Kim, K.W. Park, S. Jung, M.D. Kurkuri, H.Y. Jung, *International Journal of Hydrogen Energy*, 42 (2017) 4415–4433.
6. K.C. Neyerlin, W. Gu, J. Jorne, H.A. Gasteiger, *Journal of The Electrochemical Society*, 153 (2006) A1955-A1963.
7. M.A. Garcia-Contreras, M. Gonzalez-Muñoz, *International Journal of Electrochemical Science*, 16 (2021) 1–19.
8. X. Cheng, L. Challier, A. Etcheberry, V. Noël, H. Perez, *International Journal of Electrochemical Science*, 7 (2012) 6247–6264.
9. Y. Ono, T. Mashio, S. Takaichi, A. Ohma, H. Kanasaka, K. Shinohara, *Journal of The Electrochemical Society*, 28 (2010) 69–78.
10. J.P. Owejan, J.E. Owejan, W. Gu, *Journal of The Electrochemical Society*, 160 (2013) F824–F833.
11. R. Makharia, ASME 8th International Fuel Cell Science, Engineering & Technology Conference: Brooklyn, NY, (2010).
12. N. Nonoyama, S. Okazaki, A.Z. Weber, Y. Ikogi, T. Yoshida, *Journal of The Electrochemical Society*, 158 (2011) B416-B423.
13. K. Kudo, R. Jinnouchi, Y. Morimoto, *Electrochimica Acta*, 209 (2016) 682–690.
14. Y. Liu, M. W. Murphy, D. R. Baker, W. Gu, C. Ji, J. Jorne, H.A. Gasteiger, *Journal of The Electrochemical Society*, 11 (2007) 473–484.
15. T.A. Greszler, D. Caulk, P. Sinha, *Journal of The Electrochemical Society*, 159 (2012) F831–F840.
16. D.R. Baker, D.A. Caulk, K.C. Neyerlin, M.W. Murphy, *Journal of The Electrochemical Society*, 156 (2009) B991-B1003.
17. S.J. Lee, S. Mukerjee, J. McBreen, Y.W. Rho, Y.T. Kho, T.H. Lee, *Electrochimica Acta*, 43 (1998) 3693–3701.
18. H. Oh, Y. il Lee, G. Lee, K. Min, J.S. Yi, *Journal of Power Sources*, 345 (2017) 67–77.
19. X. Wang, H. Zhang, J. Zhang, H. Xu, X. Zhu, J. Chen, B. Yi, *Journal of Power Sources*, 162 (2006) 474–479.
20. T.R. Ralph, G.A. Hards, J.E. Keating, S.A. Campbell, D.P. Wilkinson, M. Davis, J. St-Pierre, M.C. Johnson, *Journal of The Electrochemical Society*, 144 (1997) 3845–3857.
21. S. Liu, S. Li, R. Wang, Y. Rao, Q. Zhong, K. Hong, M. Pan, *Journal of the Electrochemical Society*, 166 (2019) F1308–F1313.
22. Z.H. Wan, Q. Zhong, S.F. Liu, A.P. Jin, Y.N. Chen, J.T. Tan, M. Pan, *International Journal of Energy Research*, 42 (2018) 2225–2233.
23. K. Kudo, T. Suzuki, Y. Morimoto, *Journal of The Electrochemical Society*, 33 (2010) 1495–1502.
24. S. Shen, X. Cheng, C. Wang, X. Yan, C. Ke, J. Yin, J. Zhang, *Physical Chemistry Chemical Physics*, 19 (2017) 26221–26229.